ACS OMEGA

Open Access

http://pubs.acs.org/journal/acsodf

Article

Fabrication of Hybrid Epoxy Composites (Joint Compound Adhesive) for Aluminum Substrate Applications and Their Evaluation for Mechanical Properties

Mohammad Asif Alam, Ubair Abdus Samad, Hany S. Abdo,* Arfat Anis, Ibrahim A. Alnaser, Ahmed Hassan, and Saeed M. Al-Zahrani

Cite This: *ACS Omega* 2024, 9, 39452−39463

Read Online

ACCESS | Metrics & More | Article Recommendations

ABSTRACT: This research endeavor deals with the development of an epoxy hybrid nanocomposite using aliphatic diglycidyl ether of a bisphenol A (DGEBA) epoxy matrix. The formulation used the stoichiometric ratio of the curing agent and incorporated nanopigments such as zirconium and silica, along with other microfillers. We incorporated Zr and SiO_2 nanoparticles and various other additives in the epoxy matrix and ensured homogeneous dispersion by using sonication methodology along with silane as a coupling agent. Aluminum molds were utilized to fabricate dumbbell-shaped ASTM standard samples for the testing of mechanical properties. The adhesive properties were evaluated through standard lap shear tests. Fourier transform infrared spectroscopy was utilized to analyze the cross-linking reaction of the epoxy moiety and the polyamidoamine adduct curing agent. Further characterization using field emission scanning electron microscopy, energy-dispersive spectroscopy, and high-resolution transmission electron microscopy confirmed the presence and uniform dispersion of the fillers and nanopigments. The results showed good enhancements in ultimate tensile strength, yield strength, and elastic modulus of 95.3, 162.1, and 425.4%, respectively, compared to formulations using only SiO_2. The addition of ZrO_2 and SiO_2, along with various microfillers, such as talc and aluminum silicate, led to significant improvements in the mechanical properties. This study demonstrates the synergistic efficiency of combining SiO_2 and ZrO_2 along with microfillers, such as talc and aluminum silicate, in epoxy resin for diverse applications in the construction industry, where mechanical strength and substrate adhesion are crucial.

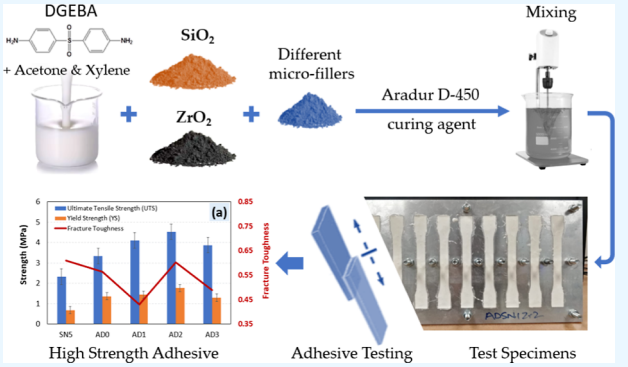

1. INTRODUCTION

Epoxy's chemical resistance and high adhesion to metals have prime significance for various applications. Because of their numerous benefits, high-performance epoxy coatings may accomplish corrosion resistance, tensile strength, outstanding thermal stability, and tribological qualities in a wide range of industrial applications.[1] Therefore, enhancement of the mechanical properties of epoxies is a contemporary approach, and strategy and efforts have been carried out by various research institutions to develop suitable coatings.[2,3] The incorporation or functionalization of inorganic fillers and pigments into the epoxy matrix improves its strength, corrosion resistance, stiffness, and chemical resistance, as demonstrated by a number of recent results and research.[4,5]

For many years, it was demonstrated that incorporating a second microphase of dispersed rubbery particles into epoxy polymers may significantly boost their toughness. Such studies were conducted by a group of scientists where they incorporated hydroxylated liquid rubber in an epoxy matrix and epoxidized natural rubber to make an epoxy blend, while curing was performed in the presence of an accelerator. This inclusion greatly improved the tensile, flexural toughness, and impact characteristics without affecting other qualities.[6−10] The performance of such multiphase thermosetting polymers has been tremendously improved, which is about 5−20% for increasing further the mechanical strength, due to the additional formation of a nanophase structure of rigid particles of silica as shown and revealed during this research.[11] The high-performance nanocomposite adhesives have been produced by incorporating zirconium oxide, ZrO_2, by weight ratio (0, 1, 3, 5, 7, and 9) % with epoxy resins and may be used to fix gaps in building walls and concrete ceilings. The results of the

Received: March 28, 2024
Revised: August 29, 2024
Accepted: August 30, 2024
Published: September 10, 2024

mechanical and adhesion tests revealed that the inclusion of zirconium enhanced the specifications of the epoxy resin. By increasing the proportion of ZrO_2 to 5%, the strength of the nanocomposite adhesive improved in tensile and impact tests, shear bonding and pull-off tests, and thermal expansion.[12] Due to the brittle behavior, failure, and thermal degradation of epoxy adhesives, efforts have been made to incorporate nanopigments and micropigments in order to provide a viable solution for the industries. The high-performance epoxy adhesives were developed with phenolic resin blend with an epoxy matrix and alumina microparticles in order to achieve tensile, single-lap joint, and thermogravimetric properties of epoxy adhesive. The results showed that adding 40% alumina microparticles, 15% recycled tire powder, and 30% phenolic resin to epoxy resulted in an 80% increase in lap shear strength over plain epoxy. The nanopigments-incorporated epoxy adhesives enlightened and led the future perspective of research in this field.[13] Taguchi experimental design approach and research were applied to solve the drawback of the brittle behavior, thermal stability of epoxy as an adhesive for metal−polymer interfaces, by incorporating clay nanoplatelets.[9] The major impacts of nanopigments on mechanical characteristics of epoxy adhesives such as tensile strength, Young's modulus, and toughness were documented, with a 39% increase in single-lap shear strength compared to blank epoxy glue without any nanopigment nanoclay. The crack mechanism in the form of deviation of crack growth pathway was investigated by field emission scanning electron microscopy (FE-SEM) when incorporated with large platy nanopigments (clay). The degradation peak temperature monitoring revealed the improvement in thermal stability for the developed epoxy adhesive.[14]

The author revealed the research on high-performance adhesives with epoxy resins containing nanofillers which are extensively applied in exterior car body panels, aircraft, and marine environments. This research also demonstrated the properties of nanostructured epoxy-based materials.[15−17] To obtain particular qualities such as conductivity for industrial applications, several epoxy nanocomposites including CNTs, graphene, carbon black, fumed silica, barium titanate, and calcium copper titanite have been produced.[18−21] Nanocomposites based on an epoxy matrix and functionalized with zirconia (ZrO_2) nanoparticles (1−3 wt %) have been developed and examined by energy-dispersive X-ray spectroscopy (EDS), FE-SEM, Fourier-transform infrared (FTIR) spectroscopy, thermogravimetric analysis (TGA), elastic modulus, and microhardness measurement with the nanoindentation. The corrosion stability during immersion in a 3.5% NaCl solution was measured by electrochemical impedance spectroscopy, and the findings indicated that the coating combined with 2% ZrO_2 had greater corrosion stability and adhesion than the clean epoxy.[22] The manufactured epoxy coatings, combined with the synergistic combination of SiO_2 and ZrO_2, showed significant improvements in the ultimate tensile strength (UTS), yield strength (YS), and elastic modulus. When compared to SiO_2-based epoxy coating alone, the composition of both ZrO_2 and SiO_2 led to significant increases of 43.5% in UTS, 74.2% in YS, and 8.2% in the elastic modulus. The developed coating and research revealed an improvement in the anticorrosion efficiency of SiO_2 and ZrO_2-incorporated nanocomposite coating in hybrid combination for various industrial applications.[23]

Various formulations have been developed and characterized during this research based on the research and findings of the epoxy-based adhesives' performance and their suitability for specific application by the incorporation of appropriate ingredients and nanofillers.[22,23] In the present research work, microfillers such as aluminum silicate, titanium dioxide, and fumed silica along with the proper curing with resin blend have been fabricated and characterized in order to use the final product as an epoxy adhesive for industrial applications.

2. MATERIALS AND METHODS

DGEBA-type epoxy resin and Aradur D-450 curing agent were procured from Hexion Chemicals, Iserlohn, and Huntsman Advanced Materials, Deutschland, Germany. The additives were purchased from BYK Additives & Instruments Company, Germany. The solvents needed to ease mixing, such as acetone and xylene, were acquired locally from Ideal Chemicals in Riyadh, Saudi Arabia. The nanoparticles employed in this investigation, such as silica (10−20 nm particle size) and ZrO_2 (<100 nm particle size), were obtained from Sigma-Aldrich under the catalog numbers 637238 and 544760, respectively. Other fillers, according to Table 1, were procured locally.

Table 1. Formulation Ingredients According to Their Addition Sequence (Values in g)

adhesive formulation	AD0	AD1	AD2	AD3
epoxy	83.34	83.34	83.34	83.34
xylene	4.5	4.5	4.5	4.5
[a]BYK additives (%)	0.6−1.5	0.6−1.5	0.6−1.5	0.6−1.5
rheology agent	0	2	2	2
fumed silica	0	3	3	3
microfillers	0	63	63	63
dispersed nanoparticle mixture (SiO_2/ZrO_2)	5:2	1:2	3:2	5:2
compatibilizer	0	2	2	2
formaldehyde resin	0	0.5	0.5	0.5
hardener	16.66	16.66	16.66	16.66

[a]104 s (0.6%), 9076 (1.5%), 333 (1%), 530 (1%).

In more detail, the BYK additives include the following: (a) BYK-9076 dispersing agent, which is responsible for suitable and better dispersion for high-performance solvent-based systems, and (b) BYK P-104 silicone-based antifoaming agent, which controls bubble formation on the coating surface. Furthermore, urea formaldehyde resin B101 was used to enhance the mechanical performance of the produced adhesive due to its excellent bonding capabilities and improvement of durability and structural integrity. The formulation also includes microfillers such as titanium dioxide (TiO_2), purchased from the National Titanium Dioxide Company (Crystal), Saudi Arabia, with an average particle size of 50 μm. To improve the quality of the adhesive, Egyptian talc was used. This talc, primarily composed of magnesium and silicon in plate-like particles, provides a smooth feel and improves the mechanical properties and stability of the produced coating. The silane used as a compatibilizer to enhance the dispersion of nanopigments in adhesive formulations is (GLYMO) 3-glycidyloxypropyltrimethoxysilane, purchased from Evonik Industries, Germany. To achieve thixotropic or rheological properties, Bentone SD-1, a type of organoclay used to modify the flow properties of liquid systems, was utilized.

https://doi.org/10.1021/acsomega.4c02971
ACS Omega 2024, 9, 39452−39463

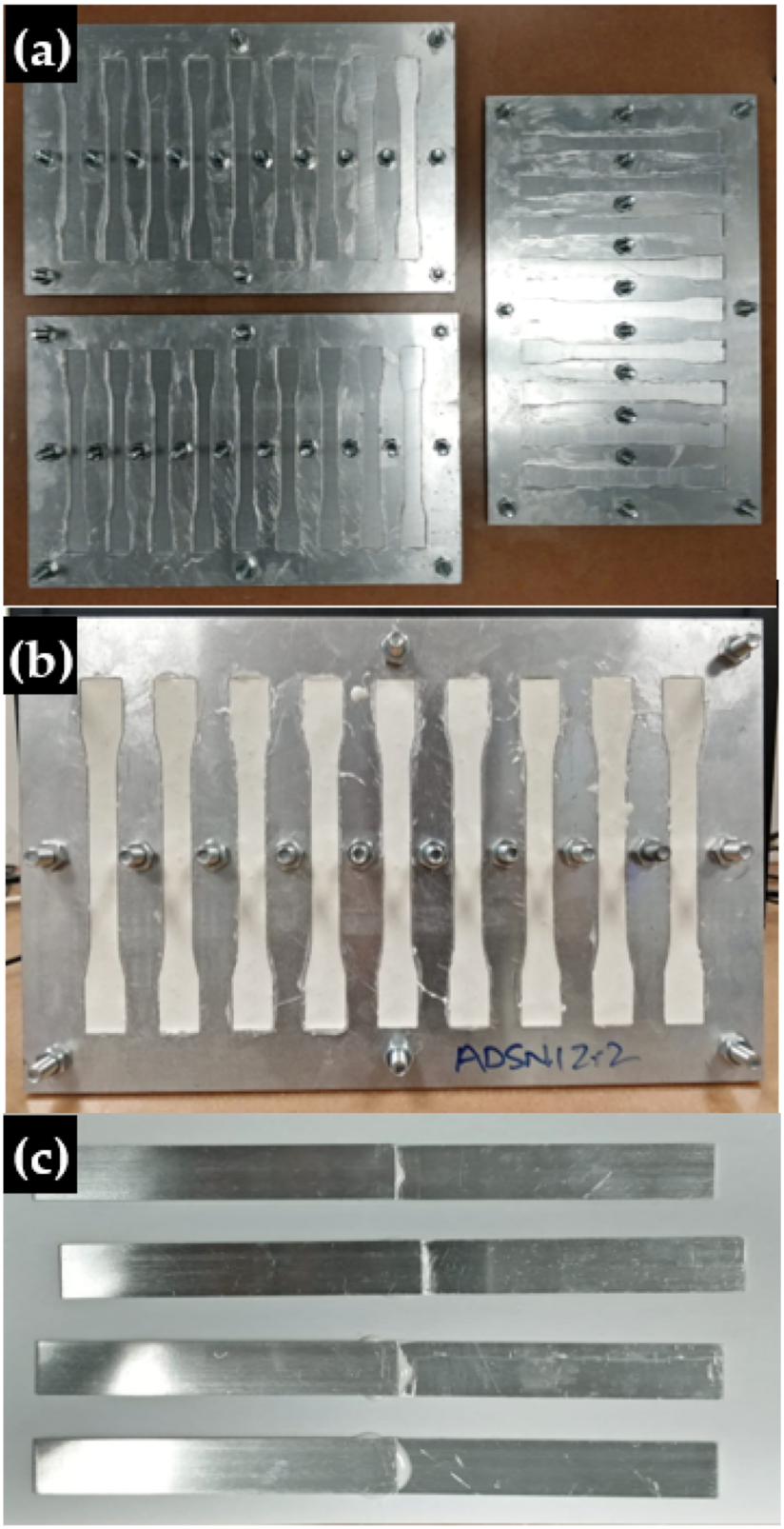

Figure 1. (a) Dog bone-shaped molds for sample preparation, (b) filled mold with samples, and (c) lap sheer samples.

The formulations were prepared using a stoichiometric balance of a hardener and epoxy. The resin was initially put in a beaker and diluted with the help of xylene using a mechanical stirrer (Sheen S2 dispersion master, Sheen instruments, Surrey, UK), as described in our earlier published paper.[24] To guarantee adequate mixing or nanopigments with the resin, the NPs were disseminated using sonication in acetone containing silane (GLYMO). The nanoparticle mixture was sonicated for 30 min. On the other hand, the addition of fillers was done in sequence, as presented in Table 1. After the

https://doi.org/10.1021/acsomega.4c02971
ACS Omega 2024, 9, 39452−39463

addition of all of the ingredients according to Table 1, the dispersed nanoparticle solution was slowly added to the prepared mixture, while the mechanical stirrer was continuously stirred at 500 rpm. Following the addition of the dispersed nanoparticle mixture, the formulation was subjected to 40−45 min of high-speed mechanical mixing at 5000 rpm to aid in dispersion and solvent removal. Once the mixing was finished, the other remaining ingredients from Table 1 were added and mixed, and a stoichiometric quantity of hardener was added to finish the formulation. The formulations were left for stabilization for a few minutes; after that, the prepared samples were poured in a dog bone-shaped mold prepared according to ASTM D 638-14 for mechanical and other characterization. To check the sheer strength, the prepared adhesive was applied between two aluminum substrate samples (prepared according to ASTM D 1002-05) and left for curing. After complete curing at room temperature, the samples were ready for characterization.

The microstructure characterization of the prepared samples was done with the help of FE-SEM to analyze the surface of the fractured sample. High-resolution transmission electron microscopy was used to confirm the presence of nano- and microfillers in the epoxy matrix. EDS was also performed along with scanning electron microscopy (SEM) for elemental analysis of the ingredients added to the complete formulation. Transmission electron microscopy (TEM) for the prepared sample was done using a JEOL (Model JEM-2100F). The samples were prepared by using an ultramicrotome (Micro star technology, USA). The samples were cut into thin slices using a MS1 microtome slicer with the help of a diamond knife. The sample was mounted on the slicer, and very thin slices in the nanometer range were produced using the automatic slicing function.

FTIR spectroscopy was performed on the prepared samples to detect the changes or formation of new bonds with the introduction of fillers and nanoparticles. The samples were scanned from 400 to 4000 cm^{-1}.

The Q600 thermal analyzer from TA Instruments (New Castle, DE, USA) was used to study the degradation profile and the influence of nanoparticles and fillers on decomposition temperatures. All samples were heated in a nitrogen atmosphere from room temperature to 600 °C using a ramp control with a ramping rate of 10°/min.

The mechanical characteristics of the produced samples were examined using the universal testing equipment (Figure 1). The dog bone-shaped samples were made according to ASTM D638-14[25] and ASTM D1002-05 standards[26] for tensile and shear tests, respectively.

3. RESULTS AND DISCUSSION

3.1. Fourier Transform Infrared Spectroscopy. The FTIR spectrum obtained for the prepared material is shown in Figure 2. The spectra were recorded between 400 and 4000 cm^{-1}. The dominant wide peak in the 3400 cm^{-1} area is due to NH for the amine compound and −OH stretching, which is suggestive of an epoxide ring opening reaction between the hardener and resin.[23] The band at 2936 cm^{-1} indicates symmetric stretching vibrations for $-CH_3$, whereas the band at 2873 cm^{-1} represents asymmetric stretching vibrations. Peaks at 1604 and 1510 cm^{-1} arise due to the N−H band and C−N stretching band, which conform to the interaction of epoxy and hardener (curing process); another indication is the presence of a peak at around 1480 cm^{-1}, which corresponds to the CH_2

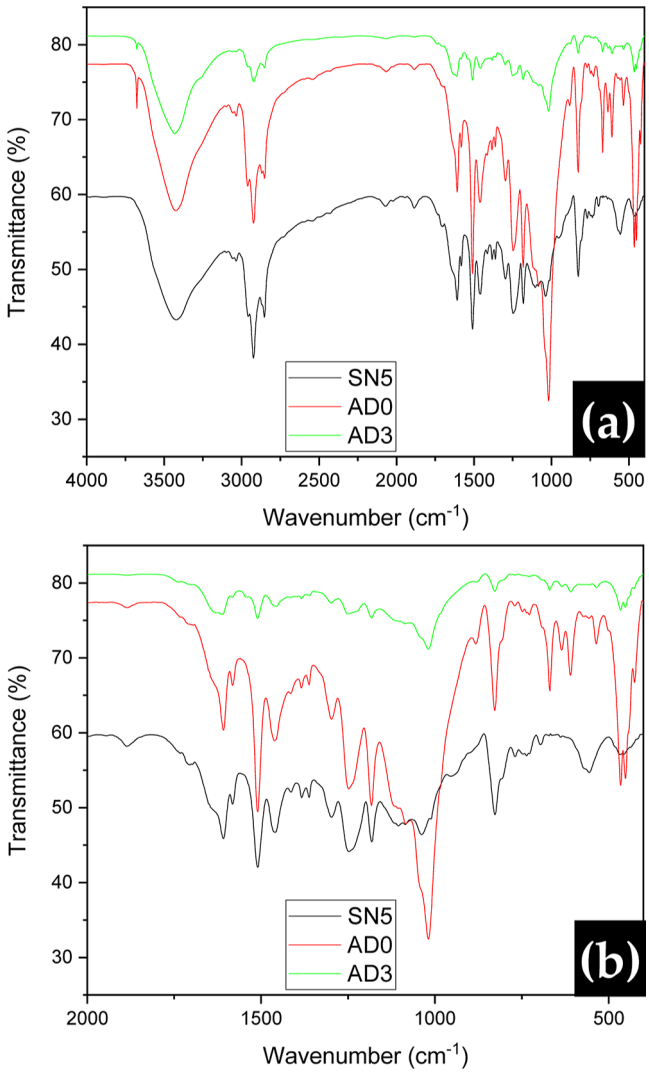

Figure 2. FTIR spectra for the (a) complete 400−4000 cm^{-1} range and (b) from 400 to 2000 cm^{-1}.

formation because of the reaction between the epoxy ring and amine of the hardener.[11] Furthermore, the peaks of the epoxy group at 3056 and 915 cm^{-1} decreased during the cross-linking process, as shown in the IR spectra.[27] The peak at 1248 cm^{-1} represents the C−O−C stretching of the aryl alkyl ether groups, which remains intact during the cross-linking process.[28] The peaks at 1095, 825, and 551 cm^{-1} correspond to the antisymmetric stretching vibration of the Si−O−Si bond, symmetric stretching vibration of the Si−O bond, and Si−O bond bending vibration, respectively. The existence of a peak at 467 cm^{-1} indicates the presence of Si−O−Si bending.[29] The characteristic peaks observed in the range of 500 cm^{-1} correspond to the stretching vibrations of Zr−O of the ZrO_2 phase, which confirms the presence of ZrO_2.[30,31]

3.2. Thermal Properties. The thermal degradation profiles of the base formulation as well as the prepared adhesive formulations are shown in Figure 3. Table 2 shows the obtained temperatures at 15, 25, and 50% weight loss, the maximum degradation temperature, and residue char at 600 °C for all the prepared formulations. The degradation behavior of the prepared samples is similar for all the formulations. As can be witnessed from the obtained weight loss vs temperature curves, the addition of microfillers for the adhesive

https://doi.org/10.1021/acsomega.4c02971
ACS Omega 2024, 9, 39452−39463

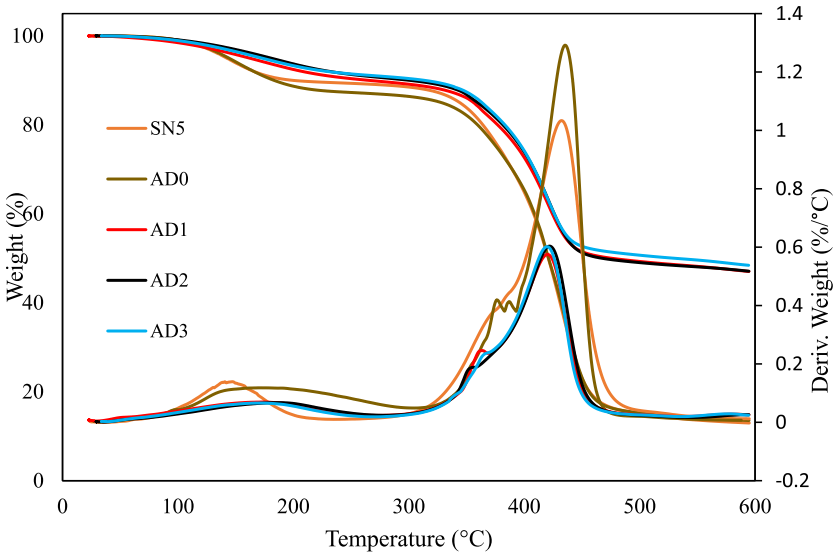

Figure 3. Obtained TGA curves of formulated samples.

Table 2. Recorded Weight Loss Temperatures at Different Percentages of Prepared Formulations

sample	T15% loss (°C)	T25% loss (°C)	T50% loss (°C)	T_{dmax}	residue (%)
SN5[33]	344.10	377.80	420.90	431.96	12.96
AD0[20]	330.19	376.04	421.54	432.23	13.52
AD1	356.15	393.82	467.48	420.19	47.03
AD2	359.61	397.18	475.75	422.53	47.09
AD3	363.36	398.97	530.35	420.37	48.43

formulations increased the capability of materials to withstand higher temperatures because of higher filler loadings.

The initial degradation phase started above 100 °C up to 300 °C. This phase accounts for the degradation of usually smaller molecules, i.e., unreacted resin and hardener components, trapped solvent molecules, etc.[13] Incorporating fillers increased the temperatures during the initial degradation stages, evidenced by higher temperatures recorded at 15% weight loss in the adhesive formulations. Beyond 300 °C, marking the onset of primary epoxy chain degradation, the adhesive samples consistently displayed significantly elevated temperatures compared with their base formulations.

The addition of microfillers significantly increased the temperature at 25% weight loss reaching up to 400 °C for all the adhesive formulations in comparison to the formulations without fillers. Meanwhile, the temperature at 50% weight loss reached above 500 °C for the AD3 samples. The reason behind this increase in temperature is the filler and matrix interaction and higher quantity of filler loadings. The higher filler ratio tends to increase the cross-link density of the resin, which in turn reduces the molecular chain mobility, thus resulting in higher thermal stability.[32] For all the prepared samples, the maximum degradation temperature (T_{dmax}) was also analyzed. As can be seen in Table 2, the maximum degradation temperature is higher for the base sample (AD0). With the incorporation of fillers, it decreased slightly; this decrease is almost 10 °C. When comparing base formulation with the formulation containing highest loading of fillers, this decrease is very negligible in comparison to the temperatures obtained at different weight loss stages, which indicates increased thermal stability. The sample SN5 represents the formulation with SiO_2 particles only.[33] However, the base formulation is the synergism of SiO_2 and ZrO_2 nanoparticles without microfillers.[23]

3.3. Mechanical Properties. *3.3.1. Tensile Behavior.* The tensile tests were carried out using an Instron 150 kN machine (Figure 4) on adhesive samples containing microfiller and

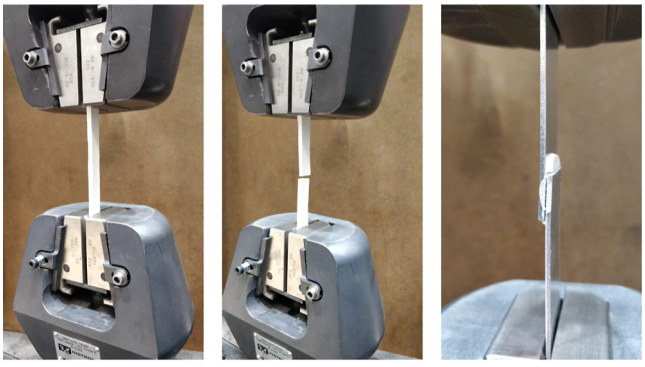

Figure 4. Tensile samples (a) attached to grip before the test, (b) fractured sample after the test, and (c) fractured lap sheer test sample.

combination on nanoparticle in varying proportions of SiO_2 and ZrO_2 to assess their mechanical characteristics. Figure 5 depicts the resulting stress−strain curves, which give useful information.

The tensile strength of polymer−nanoparticle composites is primarily determined by the properties of the polymer matrix, the reinforcement material, and the interface between them. The polymer matrix provides the structural foundation, while the reinforcement materials, such as nanoparticles and microfillers, enhance the overall strength and performance of the composite. Additionally, the interface between the polymer matrix and nanoparticles plays a crucial role in transferring stress and load between the two components.

During the tensile test, stress−strain curves are obtained, which provide valuable insights into the mechanical behavior of the composites. These curves allow us to extract important parameters, such as the YS and tensile strength. By analyzing

https://doi.org/10.1021/acsomega.4c02971
ACS Omega 2024, 9, 39452−39463

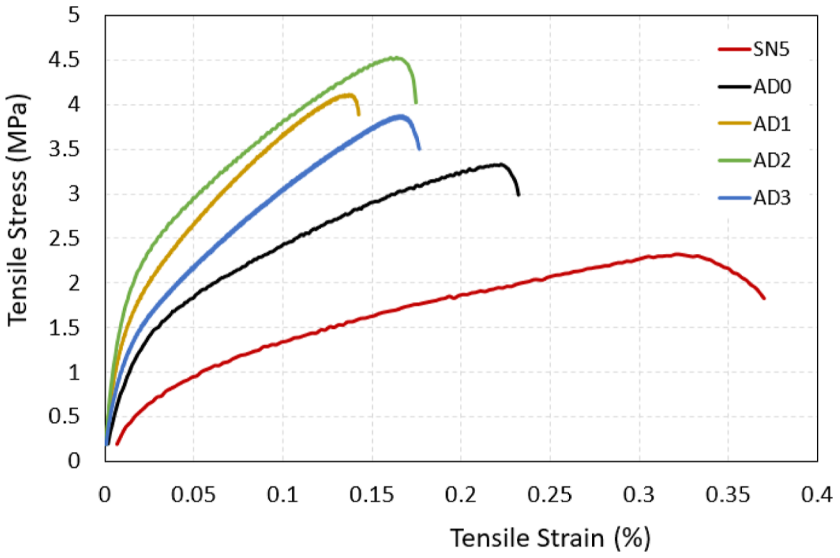

Figure 5. Tensile stress−strain curves for silica and silica/ZrO_2 and microfillers filled epoxy composites.

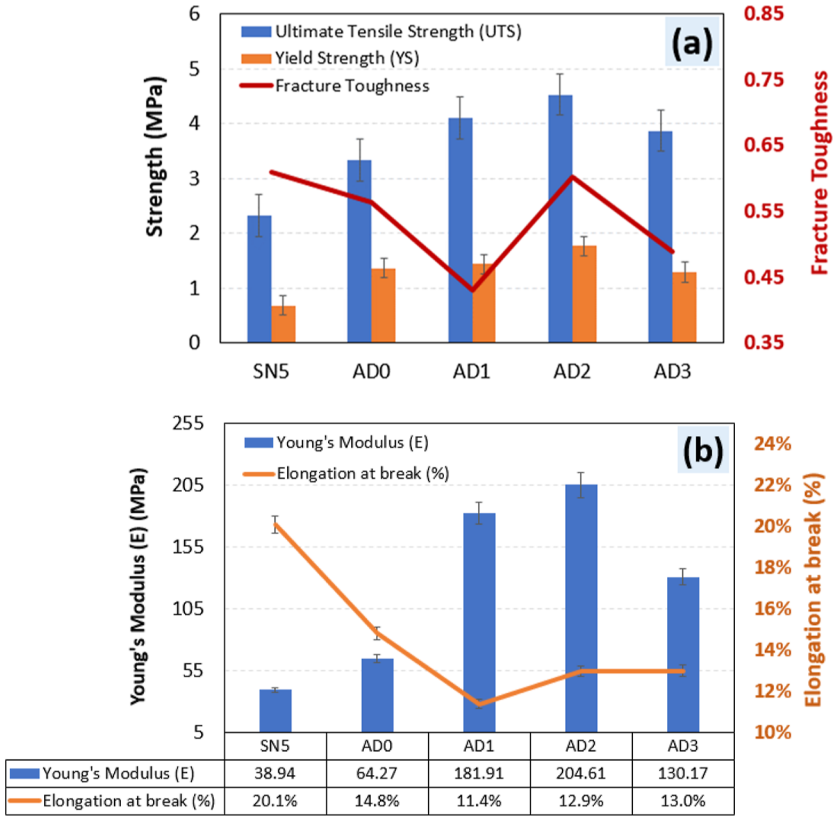

Figure 6. (a) UTS, YS, and fracture toughness and (b) Young's modulus (E) and elongation at break (%) for microfillers-filled epoxy composites.

these parameters, we can evaluate the effectiveness of different nanoparticles, such as SiO_2 and ZrO_2 along with microfillers, in enhancing the mechanical properties of the epoxy composite.

Furthermore, Figure 5 illustrates the stress−strain curves for epoxy composites with varying weight ratios of SiO_2 and ZrO_2 nanoparticles, along with microfillers in combination with nanoparticles (prepared adhesives as shown in Table 1). This visual representation enables a comparative analysis of the composites' mechanical performance as the nanoparticle content increases. This additional information assists in understanding the relationship between the nanoparticle content and the resulting tensile strength of the composite, which is a typical trade-off in this particular scenario.[34,35]

Figure 6a,b shows the results obtained from the tensile strength measurements, YS, Young's modulus, fracture toughness, and elongation at break of epoxy/SiO_2 and ZrO_2, and microfillers-filled epoxy composites highlight significant variations in their mechanical properties. Interestingly, the highest tensile strength values are observed when the SiO_2 and ZrO_2 nanoparticles are added at a 3 and 2% weight ratio, reflecting similar trends in YS and Young's modulus. However, the elongation at break exhibits an almost opposite trend, with

https://doi.org/10.1021/acsomega.4c02971
ACS Omega 2024, 9, 39452−39463

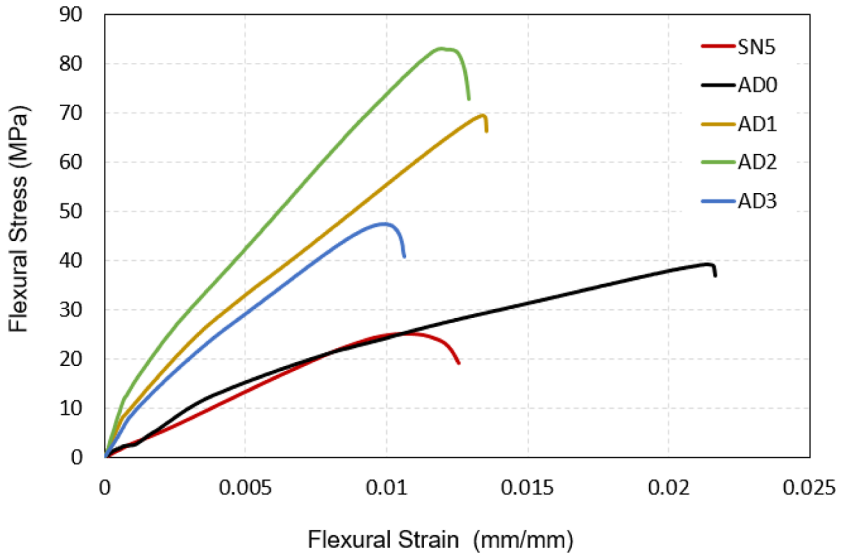

Figure 7. Curves of flexure stress−strain for silica and silica/ZrO_2-loaded epoxy coatings.

the highest values observed at lower nanoparticle concentrations. This implies that while nanoparticles enhance tensile strength, YS, and Young's modulus, they may concurrently decrease elongation at break. Beyond the optimal composition, the tensile strength, YS, and Young's modulus of the nanocomposites start to decline, aligning with the decrease in elongation at break.

This behavior can be attributed to several factors. First, the excessive addition of SiO_2 and ZrO_2 nanoparticles may lead to poor bonding within the filler material. This can result in reduced interfacial adhesion between the nanoparticles and the epoxy matrix, leading to a decrease in the overall tensile strength of the nanocomposites. It is important to carefully optimize the nanoparticle content to strike a balance between reinforcing effects and maintaining strong interfacial interactions.

The effective dispersion and distribution of nanoparticles inside the epoxy matrix result in high immobility nanolayers around each nanoparticle. This restricts the mobility of the epoxy chains, contributing to the improved mechanical properties. However, the formation of this nanoparticle network also decreases the overall mobility of the nanocomposite system. As a result, the tensile strength may start to deteriorate beyond the optimal filler/nanoparticle content.

These findings align with previous research highlighted in,[23] further supporting the understanding that the tensile strength of epoxy/SiO_2 and ZrO_2 nanocomposites is influenced by factors such as filler content, interfacial adhesion, and changes in the epoxy chain structure. Optimizing these factors is crucial for achieving enhanced mechanical properties in polymer−nanoparticle composites.

3.3.2. Shear Strength. The polymeric materials' shear strength property plays a crucial role in determining the quality of the adhesive. To assess this property, a shear test is conducted to measure how susceptible a standard test specimen is to a shear load. The test results are then expressed in terms of flexural strength and flexural strain, as shown in Figure 7.

Upon analyzing the results of the shear strength test, it was observed that the addition of ZrO_2 particles and microfillers had a positive impact on the flexural strength. Specifically, the highest strength was achieved for the AD2 sample. However, increasing the percentage of SiO_2 nanoparticles in AD3 resulted in a decrease in flexural strength.

The reduction in flexural strength arises from the robust interfacial shear strength between the filler and matrix, facilitated by cross-linking or supramolecular bonding, effectively covering or shielding the fillers and impeding fracture propagation. Additionally, a sturdy connection between the filler and the resin matrix can influence the fracture propagation behavior. In the AD3 formulation, the aggregation of modified SiO_2 and ZrO_2 results in bigger particle size, leading to a notable decline in flexural strength; this is attributed to the exacerbating stress concentration around the filler aggregates, facilitating crack propagation. Moreover, the increase in the percentage of SiO_2 and ZrO_2 particles leads to filler aggregation, thereby reducing the filler/matrix interface area, diminishing energy dissipation per unit volume, resulting in a corresponding reduction in flexural strength, consistent with our previous findings.[23] A strong interfacial adhesion between the filler and matrix is generally beneficial for improving the mechanical properties; however, an excessively high interfacial shear strength can lead to stress concentration at the interfaces and can create localized failure points, thereby reducing the overall flexural strength of the composite material. Therefore, although a robust interface is desirable, excessively high interfacial shear strength can result in unintended consequences, such as stress concentration and diminished mechanical performance.

By analyzing the stress−strain curves obtained from the shear test, we can determine the flexural strength of both epoxy/nano- and EP/nano/microfiller composites. It was observed that the maximum stress occurred for the AD2 formulation. Comparing the flexural strength of the epoxy adhesive to that of the epoxy nanocomposite, a significant improvement was noted. The flexural strength of AD2 was measured at 83 MPa. The addition of SiO_2/ZrO_2 weight ratio resulted in a notable enhancement in the flexural strength of the epoxy nanocomposites, particularly for AD2, as depicted in Figure 8.

Increased nanoparticle integration, accomplished by increasing the weight fraction, aids in the creation of a uniform and

https://doi.org/10.1021/acsomega.4c02971
ACS Omega 2024, 9, 39452−39463

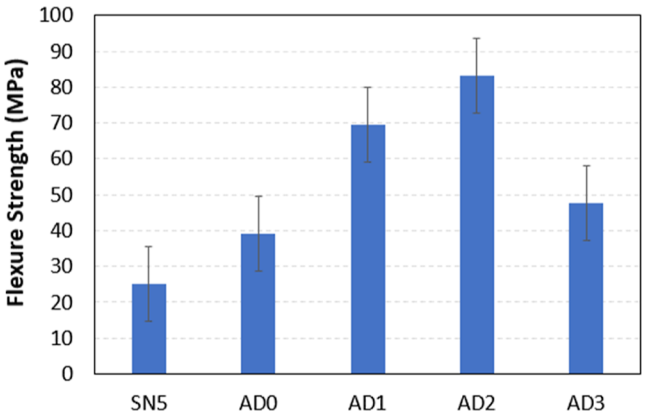

Figure 8. Flexure strength silica and silica/ZrO_2-filled epoxy coatings.

continuous surface. This contact is critical in forming a robust polymer network, which eventually improves the mechanical characteristics of the nanocomposites. The load transmission between the matrix and nanofillers is directly influenced by the quality of this interface and the strength of adhesion at the interface.

The consistency observed across various tests not only demonstrates the resilience of the sample but also affirms the reliability of the testing methods employed.[30]

3.3.3. Scanning Electron Microscopy. The SEM images provide critical insights into the textural and morphological characteristics of the adhesive samples, particularly in terms of interfacial bonding and the overall quality of the composite material. By examining the fracture surfaces following tensile testing, as shown in Figure 9, we can assess the impact of different filler loadings on the material's structure, at both low and high magnifications.

The images reveal a noticeable transformation in the morphology of the adhesive material before and after the incorporation of various fillers. Initially, the fracture surface exhibits a relatively smooth texture, indicative of a more brittle fracture typical of unfilled or lightly filled epoxy systems. However, with the introduction of higher filler loadings, the morphology shifts to a more irregular fracture pattern. This change suggests an enhanced interaction between the matrix and the fillers, which is crucial for improving the mechanical properties of the adhesive. The irregular fracture pattern, characterized by rougher surfaces and more complex crack paths, indicates stronger interfacial bonding and increased resistance to crack propagation due to the presence of fillers.

Figure 2i focuses on the specific area of the adhesive formulation AD-3, where elemental analysis was conducted by using EDS. This analysis is vital as it confirms the composition and distribution of the various elements within the adhesive. The EDS results, presented in Figure 9j, align well with the expected composition based on the materials incorporated into the formulation. The detection of elements corresponding to the added fillers, such as silicon from SiO_2 and zirconium from ZrO_2, provides further confirmation of their successful integration into the adhesive matrix.

The SEM analysis, coupled with EDS, thus not only verifies the presence of the intended materials but also highlights the effectiveness of filler incorporation in altering the fracture behavior of the adhesive. This morphological evolution, from smooth to irregular fracture surfaces, underscores the critical role of fillers in enhancing the interfacial bonding and the overall mechanical robustness of the adhesive formulation.

By examining the fracture path of sample AD2, it becomes evident that a crack deflection mechanism is at play.[36,37] This process is based on the idea of greater plastic deformation happening in the system when a high density of fillers coexists with an epoxy matrix. Consequently, fractures form in sample AD2 by branching and bending around particles, which promotes plastic deformation and, as a result, increased fracture toughness, as reported in the mechanical properties in Section 3.3. While particle cavitation does occur, its role in sample AD2 is secondary to the crack deflection mechanism.

When evaluating the micrographs of sample AD3, it is discovered that the particle domain sizes imply the formation of a nearly smooth surface that is totally cavitated under stress. The particle cavitation process absorbs the energy of the external load, which is the primary explanation for the increase in the fracture toughness in sample AD3. In contrast, the signs of cavitation are minor in sample AD2 compared to AD1 and AD3, indicating that cavitation plays a lesser role in sample AD2's fracture toughness compared to the crack deflection mechanism.[14] The reduction in cavitation could be attributed to the deagglomeration of the microfiller. Deagglomeration promotes a more uniform dispersion of the filler within the matrix, resulting in improved mechanical properties and reduced cavitation formation.

3.3.4. Transmission Electron Microscopy. The obtained TEM images of the adhesive samples, as shown in Figure 10, provide detailed insights into the microstructural arrangement and distribution of the fillers within the epoxy matrix. In Figure 10a, the presence of both microsized particles, such as Talc, Blank fix micro, and TiO_2, along with nanosized particles (SiO_2 and ZrO_2), is clearly visible, indicating a uniform distribution within the adhesive formulation. This uniform dispersion is critical as it directly impacts the mechanical properties and overall performance of the adhesive.

Moving to Figure 4b, the addition of microparticles of varying sizes can be distinctly observed, further supporting the diverse particle size distribution within the adhesive. This variation in particle size is intentional as it contributes to a more complex and effective reinforcement network within the epoxy matrix, potentially enhancing the mechanical properties of the adhesive.

To confirm the incorporation and distribution of the nanoparticles within the adhesive, we reduced the imaging scale to the nanometer range. Figure 10c,d specifically highlights the presence of SiO_2 nanoparticles, with sizes up to 20 nm, and ZrO_2 nanoparticles, with sizes under 100 nm. The presence of these nanoparticles, as confirmed by TEM, is crucial as their small size and high surface area are expected to contribute significantly to the adhesive's performance, particularly in terms of mechanical strength and durability.

However, it is worth noting that achieving an ideal dispersion of nanoparticles within the matrix is inherently challenging, especially at higher filler loadings. The observed dispersion quality, while satisfactory, is not without limitations as the higher content of fillers can lead to localized agglomeration, which may slightly compromise the uniformity of the distribution. This phenomenon is particularly evident at the highest concentrations of fillers, where the balance between achieving a high filler content and maintaining a homogeneous dispersion becomes more difficult to manage.

https://doi.org/10.1021/acsomega.4c02971
ACS Omega 2024, 9, 39452−39463

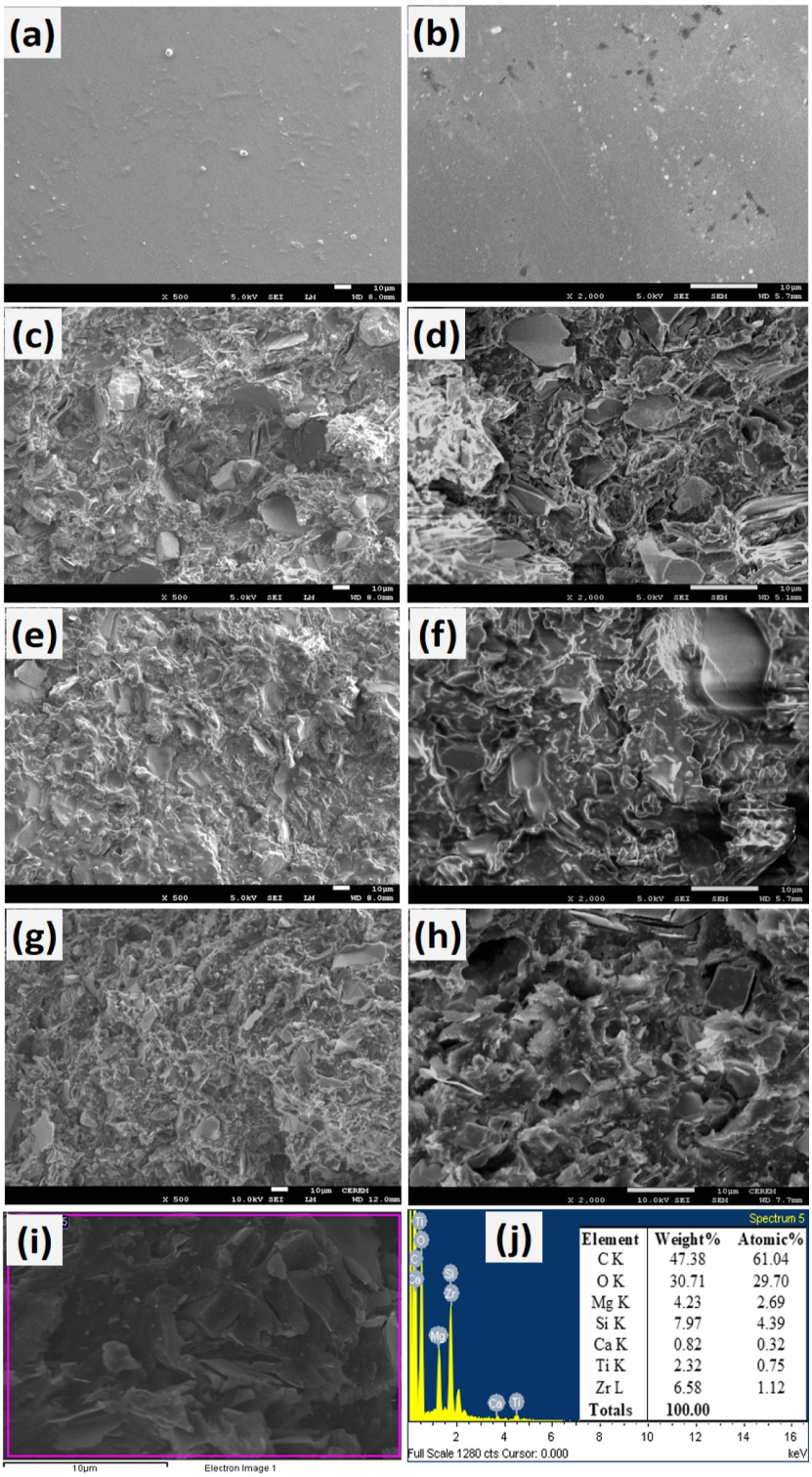

Figure 9. SEM images of the adhesive fractured surface (a,b) AD0, (c,d) AD1, (e,f) AD2, (g,h) AD3, and (i) the area where EDS was taken, and (j) EDS along with the elemental composition for AD-3 adhesive formulation.

Overall, the TEM images provide a comprehensive view of the filler distribution within the adhesive, confirming the successful incorporation of both micro- and nanosized particles, albeit with some challenges related to dispersion at higher filler concentrations. These observations underscore the complexity of optimizing the filler content and dispersion in hybrid nanocomposite formulations.

4. CONCLUSIONS

The developed hybrid nanocomposite epoxy formulations, leveraging the synergistic effects of SiO_2 and ZrO_2 nanoparticles alongside compatible microfillers, represent a significant advancement in adhesive technology applicable across diverse substrates. Through meticulous formulation, we harnessed the complementary properties of ZrO_2 and SiO_2

https://doi.org/10.1021/acsomega.4c02971
ACS Omega 2024, 9, 39452−39463

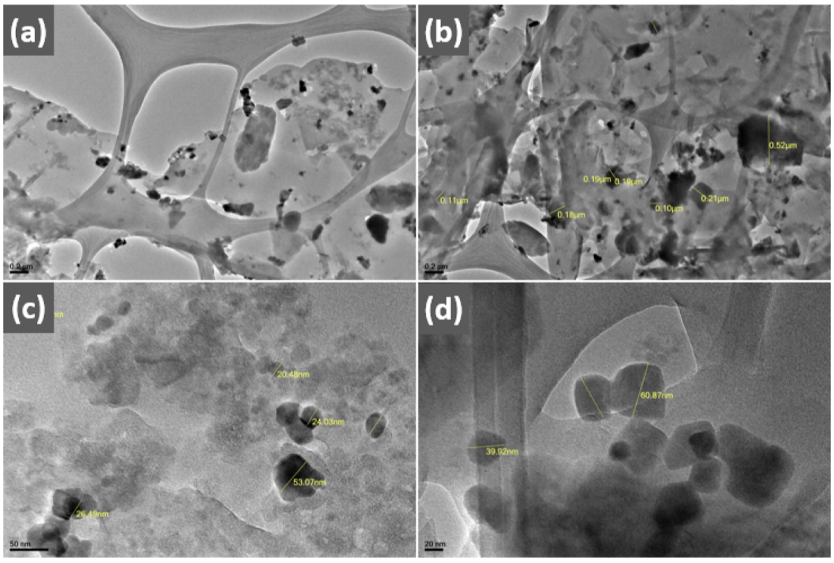

Figure 10. TEM images of the prepared sample (AD-2) at different magnifications: (a,b) 50k mag, (c) 100k mag, and (d) 200k mag.

nanoparticles, bolstered by various additives and fillers, culminating in superior mechanical performance and strength. Quantitatively, our findings underscore the efficacy of this approach. Specifically, compared to formulations utilizing only SiO_2, we observed enhancements of 95.3, 162.1, and 425.4% in UTS, YS, and elastic modulus, respectively. Incorporating both ZrO_2 and SiO_2 nanoparticles, in conjunction with microfillers and a blend of formaldehyde resin with epoxy, yielded notable enhancements in adhesive performance. Our analyses, particularly through tensile and shear strength tests, revealed a discernible positive impact on the mechanical properties. Notably, the AD2 sample exhibited the highest strength, indicative of the formulation's efficacy. However, a nuanced observation emerged regarding the AD3 sample, where an increase in the nanoparticle percentage led to a reduction in overall properties.

■ ASSOCIATED CONTENT

Data Availability Statement

The data are available throughout the manuscript and supporting files.

■ AUTHOR INFORMATION

Corresponding Author

Hany S. Abdo − *Center of Excellence for Research in Engineering Materials (CEREM), King Saud University, Riyadh 11421, Saudi Arabia;* orcid.org/0000-0002-7260-639X; Email: habdo@ksu.edu.sa

Authors

Mohammad Asif Alam − *Center of Excellence for Research in Engineering Materials (CEREM), King Saud University, Riyadh 11421, Saudi Arabia*

Ubair Abdus Samad − *Center of Excellence for Research in Engineering Materials (CEREM), King Saud University, Riyadh 11421, Saudi Arabia*

Arfat Anis − *SABIC Polymer Research Center (SPRC), Chemical Engineering Department, King Saud University, Riyadh 11421, Saudi Arabia*

Ibrahim A. Alnaser − *Mechanical Engineering Department, College of Engineering, King Saud University, Riyadh 11421, Saudi Arabia;* orcid.org/0000-0001-6325-8410

Ahmed Hassan − *Mechanical Engineering Department, College of Engineering, King Saud University, Riyadh 11421, Saudi Arabia;* orcid.org/0000-0002-6840-8999

Saeed M. Al-Zahrani − *SABIC Polymer Research Center (SPRC), Chemical Engineering Department, King Saud University, Riyadh 11421, Saudi Arabia*

Complete contact information is available at: https://pubs.acs.org/10.1021/acsomega.4c02971

Author Contributions

Conceptualization, M.A.A., U.A.S., H.S.A., A.A., and S.M.A.-Z.; methodology, U.A.S.; software, U.A.S. and H.S.A.; validation, M.A.A., A.A., and I.A.A.; formal analysis, M.A.A., U.A.S, H.S.A., I.A.A., A.H., and A.A.; investigation, M.A.A., U.A.S., H.S.A., and A.A.; resources, M.A.A., H.S.A., I.A.A., and S.M.A.-Z.; data curation, M.A.A.; writing—original draft, U.A.S., M.A.A., and H.S.A.; writing—review and editing, H.S.A., M.A.A., and A.A.; visualization, A.H. and H.S.A.; supervision, S.M.A.-Z.; project administration, S.M.A.-Z.; and funding acquisition, M.A.A. All authors have read and agreed to the published version of the manuscript.

Funding

This research was funded by Deputyship for Research & Innovation, Ministry of Education in Saudi Arabia (IFKSUDR-P108).

Notes

The authors declare no competing financial interest.

■ ACKNOWLEDGMENTS

The authors extend their appreciation to the Deputyship for Research & Innovation, Ministry of Education in Saudi Arabia for funding this research work through the project number IFKSUDR-P108.

■ REFERENCES

(1) Jiang, T.; Kuila, T.; Kim, N. H.; Ku, B. C.; Lee, J. H. Enhanced mechanical properties of silanized silica nanoparticle attached

graphene oxide/epoxy composites. *Compos. Sci. Technol.* **2013**, *79*, 115−125.
(2) Samardžija, M.; Kurtela, M.; Vuković Domanovac, M.; Alar, V. Anticorrosion and Antibacterial Properties of Al NP−Epoxy Nanocomposite Coating on Grey Cast Iron. *Coatings* **2023**, *13*, 898.
(3) Samad, U. A.; Alam, M. A.; Anis, A.; Abdo, H. S.; Shaikh, H.; Al-Zahrani, S. M. Nanomechanical and Electrochemical Properties of ZnO-Nanoparticle-Filled Epoxy Coatings. *Coatings* **2022**, *12*, 282.
(4) Javidparvar, A. A.; Ramezanzadeh, B.; Ghasemi, E. Effects of surface morphology and treatment of iron oxide nanoparticles on the mechanical properties of an epoxy coating. *Prog. Org. Coating* **2016**, *90*, 10−20.
(5) Ramezanzadeh, B.; Attar, M. M. Characterization of the fracture behavior and viscoelastic properties of epoxy-polyamide coating reinforced with nanometer and micrometer sized ZnO particles. *Prog. Org. Coating* **2011**, *71*, 242−249.
(6) Mathew, V. S.; Sinturel, C.; George, S. C.; Thomas, S. Epoxy resin/liquid natural rubber system: secondary phase separation and its impact on mechanical properties. *J. Mater. Sci.* **2010**, *45*, 1769−1781.
(7) Mathew, V. S.; George, S. C.; Parameswaranpillai, J.; Thomas, S. Epoxidized natural rubber/epoxy blends: Phase morphology and thermomechanical properties. *J. Appl. Polym. Sci.* **2014**, *131*, 131.
(8) Silva, A. A. C.; Gomes, T. I.; Martins, B. D. P.; Garcia, R. B. R.; Cividanes, L. D. S.; Kawachi, E. Y. New insights in adhesive properties of hybrid epoxy-silane coatings for aluminum substrates: effect of composition and preparation methods. *J. Inorg. Organomet. Polym. Mater.* **2020**, *30*, 3105−3115.
(9) Pramanik, S.; Karak, N. Polymer nanocomposites for adhesive, coating, and paint applications. *Properties and Applications of Polymer Nanocomposites*; Springer, 2017; pp 173−204.
(10) Alam, M. A.; Samad, U. A.; Sherif, E. S. M.; Seikh, A.; Al-Zahrani, S. M.; Alharthi, N. H.; Alam, M. Synergistic effect of Ag and ZnO nanoparticles on polyaniline incorporated epoxy/2pack coatings for splash zone applications. *J. Coat. Technol. Res.* **2019**, *16*, 835−845.
(11) Kinloch, A. J.; Lee, J. H.; Taylor, A. C.; Sprenger, S.; Eger, C.; Egan, D. Toughening structural adhesives via nano- and micro-phase inclusions. *J. Adhes.* **2003**, *79*, 867−873.
(12) Ameer, N.; Ibreheim Hussein, S. Enhanced thermal expansion, mechanical properties, and adhesion analysis of epoxy/ZrO2 nano composites. *J. Phys. Conf.* **2019**, *1279*, 012026.
(13) Aliakbari, M.; Jazani, O. M.; Sohrabian, M.; Jouyandeh, M.; Saeb, M. R. Multi-nationality epoxy adhesives on trial for future nanocomposite developments. *Prog. Org. Coating* **2019**, *133*, 376−386.
(14) Aliakbari, M.; Jazani, O. M.; Sohrabian, M. Epoxy adhesives toughened with waste tire powder, nanoclay, and phenolic resin for metal-polymer lap-joint applications. *Prog. Org. Coating* **2019**, *136*, 105291.
(15) Aradhana, R.; Mohanty, S.; Nayak, S. K. High performance epoxy nanocomposite adhesive: Effect of nanofillers on adhesive strength, curing and degradation kinetics. *Int. J. Adhes. Adhes.* **2018**, *84*, 238−249.
(16) Sancaktar, E.; Kuznicki, J. Nanocomposite adhesives: Mechanical behavior with nanoclay. *Int. J. Adhes. Adhes.* **2011**, *31*, 286−300.
(17) Wernik, J. M.; Meguid, S. A. On the mechanical characterization of carbon nanotube reinforced epoxy adhesives. *Mater. Des.* **2014**, *59*, 19−32.
(18) Tuncer, E.; Sauers, I.; James, D. R.; Ellis, A. R.; Paranthaman, M. P.; Aytuğ, T.; Sathyamurthy, S.; More, K. L.; Li, J.; Goyal, A. Electrical properties of epoxy resin based nano-composites. *Nanotechnology* **2006**, *18*, 025703.
(19) Tomasi, J. M.; King, J. A.; Klimek-McDonald, D. R.; Herline, N.; Krieg, A.; Odegard, G. M.; Miskioglu, I. Electrical, thermal, and tensile properties of cycloaliphatic epoxy/carbon black and cycloaliphatic epoxy/fumed silica nanocomposites. *2018 AIAA/ASCE/AHS/ASC Structures, Structural Dynamics, and Materials Conference*, 2018.
(20) Tang, G.; Jiang, Z. G.; Li, X.; Zhang, H. B.; Hong, S.; Yu, Z. Z. Electrically conductive rubbery epoxy/diamine-functionalized graphene nanocomposites with improved mechanical properties. *Composites, Part B* **2014**, *67*, 564−570.
(21) Wang, Q.; Dai, J.; Li, W.; Wei, Z.; Jiang, J. The effects of CNT alignment on electrical conductivity and mechanical properties of SWNT/epoxy nanocomposites. *Compos. Sci. Technol.* **2008**, *68*, 1644−1648.
(22) Alam, M. A.; Samad, U. A.; Anis, A.; Sherif, E. S. M.; Abdo, H. S.; Al-Zahrani, S. M. The Effect of Zirconia Nanoparticles on Thermal, Mechanical, and Corrosion Behavior of Nanocomposite Epoxy Coatings on Steel Substrates. *Mater.* **2023**, *16*, 4813.
(23) Samad, U. A.; Alam, M. A.; Abdo, H. S.; Anis, A.; Al-Zahrani, S. M. Synergistic Effect of Nanoparticles: Enhanced Mechanical and Corrosion Protection Properties of Epoxy Coatings Incorporated with SiO2 and ZrO2. *Polymer* **2023**, *15*, 3100.
(24) Alam, M. A.; Samad, U. A.; Seikh, A.; Mohammed, J. A.; Al-Zahrani, S. M.; Sherif, E.-S. M. Development and Characterization of PA 450 and PA 3282 Epoxy Coatings as Anti-Corrosion Materials for Offshore Applications. *Materials* **2022**, *15*, 2562.
(25) ASTM. *ASTM-D638−14 Standard Test Method for Tensile Properties of Plastics*; ASTM Stand, 2014; Vol. *8*, pp 59−67.
(26) D6412, A. D6412/D6412M Standard Specification for Epoxy (Flexible) Adhesive For Bonding Metallic And Nonmetallic Materials. 2023, https://www.astm.org/d6412_d6412m-99r20.html (accessed on July 12, 2023).
(27) Nikolic, G.; Zlatkovic, S.; Cakic, M.; Cakic, S.; Lacnjevac, C.; Rajic, Z. Fast Fourier Transform IR Characterization of Epoxy GY Systems Crosslinked with Aliphatic and Cycloaliphatic EH Polyamine Adducts. *Sensors* **2010**, *10* (1), 684−696.
(28) (a) Wang, Y.; Cui, X.; Ge, H.; Yang, Y.; Wang, Y.; Zhang, C.; Li, J.; Deng, T.; Qin, Z.; Hou, X. Chemical Recycling of Carbon Fiber Reinforced Epoxy Resin Composites via Selective Cleavage of the Carbon−Nitrogen Bond. *ACS Sustainable Chem. Eng.* **2015**, *3* (12), 3332−3337. (b) Jia, Z.; Hong, R. Anticorrosive and photocatalytic properties research of epoxy-silica organic−inorganic coating. *Colloids Surf., A* **2021**, *622*, 126647.
(29) Horti, N. C.; Kamatagi, M. D.; Nataraj, S. K.; Wari, M. N.; Inamdar, S. R.; ChenBaran, Y. M.; et al. Structural and optical properties of zirconium oxide (ZrO2) nanoparticles: effect of calcination temperature. *Nano Express* **2020**, *1*, 010022.
(30) Kumar, S.; Bhunia, S.; Ojha, A. K. Effect of calcination temperature on phase transformation, structural and optical properties of sol−gel derived ZrO2 nanostructures. *Phys. E* **2015**, *66*, 74−80.
(31) Zhang, R.; Wang, H.; Wang, X.; Guan, J.; Li, M.; Chen, Y. Rubber-Composite-Nanoparticle-Modified Epoxy Powder Coatings with Low Curing Temperature and High Toughness. *Polymer* **2022**, *15*, 195.
(32) Kumar, R.; Mishra, A.; Sahoo, S.; Panda, B. P.; Mohanty, S.; Nayak, S. K. Epoxy-based composite adhesives: Effect of hybrid fillers on thermal conductivity, rheology, and lap shear strength. *Polym. Adv. Technol.* **2019**, *30*, 1365−1374.
(33) Alam, M. A.; Abdus Samad, U.; Alam, M.; Anis, A.; Al-Zahrani, S. M. Enhancement in Nanomechanical, Thermal, and Abrasion Properties of SiO2 Nanoparticle-Modified Epoxy Coatings. *Coatings* **2020**, *10*, 310.
(34) Long, J.; Li, C.; Li, Y. Enhancement of Mechanical and Bond Properties of Epoxy Adhesives Modified by SiO2 Nanoparticles with Active Groups. *Polymer* **2022**, *14*, 2052.
(35) Gershoni, G.; Dodiuk, H.; Tenne, R.; Kenig, S. Cationically Polymerized Epoxy and Radiation-Cured Acrylate Blend Nanocomposites Based on WS2 Nanoparticles Part B: Mechanical and Physical Properties. *J. Compos. Sci.* **2023**, *7*, 42.
(36) Zhao, S.; Schadler, L. S.; Duncan, R.; Hillborg, H.; Auletta, T. Mechanisms leading to improved mechanical performance in nanoscale alumina filled epoxy. *Compos. Sci. Technol.* **2008**, *68*, 2965−2975.

https://doi.org/10.1021/acsomega.4c02971
ACS Omega 2024, 9, 39452−39463

(37) Pawlak, A.; Galeski, A. Plastic deformation of crystalline polymers: The role of cavitation and crystal plasticity. *Macromolecules* **2005**, *38*, 9688−9697.

https://doi.org/10.1021/acsomega.4c02971
ACS Omega 2024, 9, 39452−39463